Effect of Molecular Architecture on Phase Behavior of Graft Copolymers

Liangshun Zhang, Jiaping Lin,* and Shaoliang Lin

Key Laboratory for Ultrafine Materials of Ministry of Education, School of Materials Science and Engineering, East China University of Science and Technology, Shanghai 200237, China

Received: March 31, 2008; Revised Manuscript Received: May 15, 2008

Influence of molecular architecture on phase behavior of graft copolymer melts was studied by using a reciprocal-space self-consistent filed theory (SCFT). The phase diagrams were examined as functions of the architectural parameters describing the graft copolymers (i.e., the number of grafts and the position of first junction). In comparison with the well-known phase diagram of diblock copolymers, the phase diagrams of the graft copolymers are asymmetric. When the number of grafts or the position of first junction varies, the boundaries of order-order transitions have shifts due to the variation in the chain stretching energy. The change in molecular architecture also significantly alters the domain spacing of ordered structures but has weak impact on the density distributions of graft copolymers. For comparison of the theoretical predictions with the existing experimental results, the phase diagrams of graft copolymers were also calculated at strong segregation. The SCFT calculations can accurately capture the characteristics of the phase behavior of graft copolymer melts.

Introduction

The most important principles of block copolymer phase behavior have been already captured by the simplest AB diblock architecture.[1–5] The microphase-separated structures of block copolymers are controlled by the delicate competition between the interaction energy and the chain stretching energy. The repulsion between the chemically different fragments drives the system to undergo phase separation; however, because the incompatible blocks are chemically connected, the system exhibits microphase separation and self-organizes into various ordered structures. For the simplest diblock copolymer melt, the ordered structures include lamella, bicontinuous gyroid, hexagonally packed cylinders, and body-centered cubic spheres. These equilibrium morphologies can be tailored by varying the copolymer composition f and the segregation degree χN between the two blocks (χ is the Flory−Huggins interaction parameter and N is the degree of polymerization).

Because of the ongoing interest in novel macromolecular organization, well-defined nonlinear copolymers with complex architectures such as graft, starblock, miktoarm, and hyperbranched copolymers have been studied experimentally.[6–10] It is shown that the molecular architecture is an important factor for tailoring the morphologies, phase behavior, and material properties. Among these copolymers with complex architecture, considerable attention has been paid to the microphase separation of graft copolymers because of their unique material properties and their applications as interface compatiblizers, thermoplastic elastomers, and viscosity modifiers.[11–13] Gido, Hadjichristidis, Mays et al. synthesized a series of architecturally well-defined graft copolymers with a polyisoprene (PI) backbone and polystyrene (PS) graft chains.[14–21] Well-ordered lamellar, cylindrical, and spherical morphologies are observed. The morphologies of graft copolymers and domain spacing of ordered structures depend on the molecular architecture of graft copolymers, such as the number of grafts and the distribution of junctions. There is a dramatic shift in the phase boundaries of graft copolymer melts compared with diblock copolymers at the given segregation degree. To predict and interpret the architectural effect on the self-assembly behavior of graft copolymers, Gido et al. proposed a constituting block copolymer hypothesis.[14–16] According to the hypothesis, the phase behavior of graft copolymers is dictated by the behavior of constituting block copolymers, which are formed by imaging all looped and bridged blocks of backbone to be cut in half. Existing Milner's theory for star copolymers is used to predict the phase boundaries of the constituting block copolymers.[22] The results of experimental studies for graft copolymers are in general agreement with the predictions of Milner's phase diagram for the constituting block copolymers. However, the Milner's phase diagram has a tendency to overestimate the copolymer composition for the order-order transitions.

A variety of theoretical methods have been used to investigate the effect of molecular architecture on the phase behavior of graft copolymers.[23–31] Olvera de la Cruz and Sanchez utilized random phase approximation (RPA) to study the order−disorder transition (ODT) of graft copolymers.[23] The calculations indicated that the spinodal value $(\chi N)_s$ of symmetric graft copolymers has a larger value compared with $(\chi N)_s$ of corresponding diblock copolymers. In a related study, Balazs and co-workers investigated the microphase separation of graft copolymers with even or random distributions of junctions.[24,25] They found that it is the χN value of the average constituting single graft copolymers which determines the proximity to the ODT. Chakraborty and co-workers developed a Landau field-theoretical model to study microphase separation in melts of randomly grafted copolymers.[26–28] The stability regions of ordered phases strongly depend on the architectural parameters, such as the backbone length, the branch length, and the number of branches. Recently, Patel and Fredrickson constructed a field theory model of randomly graft copolymer melts.[29] They carried out simulations of field theory for quenched and annealed cases by invoking the mean-field approximation. The main focus of their work was to clarify the conditions for which quenched

* Corresponding author. Tel: +86-21-64253370. Fax: +86-21-64253539. E-mail: jplinlab@online.sh.cn.

10.1021/jp802770z CCC: $40.75
Published on Web 07/17/2008

and annealed averages can be interchanged. These theoretical studies mentioned above mainly concentrate on the difference between graft copolymers and linear block copolymers. However, so far, one major unresolved issue regarding the graft copolymers is that the phase diagrams are not mapped out.

The self-consistent field theory (SCFT) has emerged as a powerful tool to study the equilibrium thermodynamical features of polymers. The theory for polymer melts has its origin from the field theoretical approach of Edwards in the 1960s.[32] Helfand and others explicitly adapted the theory to tackle the self-assembly behavior of block copolymers in subsequent decades.[33–36] Recently, Matsen and Schick developed a state-of-the-art numerical approach to solve the SCFT equations.[3,37,38] In this method, a set of basis functions based on the assumed morphological symmetries are adopted to expand the fields. The Matsen−Schick approach is suited for the accurate calculations of free energy and the construction of phase diagrams. The phase diagrams of broad class of copolymer architectures have been mapped out by performing the SCFT calculations in reciprocal space.[39–48] For example, Matsen and Schick examined the phase diagrams for melts of starblock copolymers with one, three, five, and nine arms.[39] There is a preference for the inner blocks of the arms to be located in the inside of cylindrical and spherical phases. The preference increases with increasing number of arms. Grason and Kamien performed the self-consistent field theory for melts of star copolymers or multiply branched copolymers.[46–48] Compared with the phase behavior of AB block copolymers, the phase boundaries for these copolymer melts are asymmetric. An alternative numerical approach to solve the SCFT equation was implemented in real space by Fredrickson et al.[49–51] A prior assumption about the mesophase symmetry is not necessary. This method is found to be an efficient way to screen for new types of microstructures. In our previous work, we utilized the SCFT solved in real space to study the morphologies and bridging properties of graft copolymers in the bulk and aggregate morphologies of amphiphilic graft copolymers in dilute solution.[52,53] In our model, the graft copolymers exhibit two distinctive architectural parameters: the number of grafts and the distribution of junctions. The morphological transitions can be triggered by varying the molecular architecture of graft copolymers. However, the thorough investigation on the phase behavior of graft copolymers was not carried out.

The purpose of the present work is to systemically examine the phase behavior of graft copolymers by using a reciprocal-space SCFT approach. The architectural parameters, which are the number of grafts and the distribution of junctions, were incorporated in the model of graft copolymers. The phase diagrams for graft copolymers with various values of graft number and distribution of junctions were mapped out to determine the relationship between the phase behavior and molecular architecture. It was found that the variation in molecular architecture of graft copolymers can cause shifts in the phase boundaries and change the symmetry of phase diagrams. We also examined the effect of molecular architecture on the domain spacing of ordered structures and density distribution of graft copolymers. The theoretical predictions were compared with the existing experimental results, and a good agreement was exhibited. We expect that the present study may offer a fundamental insight about the molecular architecture effect on the self-assembly behavior of graft copolymers.

Theoretical Framework

For a canonical ensemble, n_G graft copolymers are contained in a volume V. The molecular architecture of graft copolymers is shown in Figure 1. z flexible homopolymer graft chains are spaced along a flexible homopolymer backbone. The backbone and graft chain are composed of N_A A segments and N_B B segments, respectively. Therefore, the number of total segments for single graft copolymer is $N_G = N_A + zN_B$. The A or B segment occupies a fixed volume ρ_0^{-1}, so that the total volume of the system with incompressibility equals to $n_G N_G/\rho_0$. The statistical segment length a is assumed to be the same for both segments. The volume fraction of the A-type segment in the system is denoted by f_A, and that of B-type segment is $f_B = 1 - f_A$. The ith junction point is located at τ_i given by

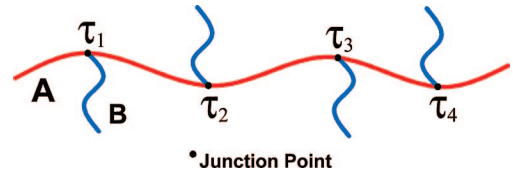

Figure 1. Molecular architecture of the graft copolymer.

$$\tau_i = \tau_1 + \frac{(i-1)(1-2\tau_1)}{z-1} \qquad 1 \le i \le z \tag{1}$$

For the Gaussian chain model adopted in the present study and within the mean-field approximation, the statistics of the polymers is modeled by the configuration of the single polymer chain, which is determined by a set of effective chemical potential fields $\omega_K(\mathbf{r})(K = A, B)$, replacing the actual interactions within the bulks. These chemical potential fields are conjugated to the segment density fields $\phi_K(\mathbf{r})$. For such an A-g-B$_z$ melt, the free energy per chain is given by

$$\frac{F}{n_G k_B T} = -\ln\frac{Q_G}{V} + \frac{1}{V}\int \mathrm{d}\mathbf{r}[\chi_{AB}N_G\phi_A(\mathbf{r})\phi_B(\mathbf{r}) - \omega_A(\mathbf{r})\phi_A(\mathbf{r}) - \omega_B(\mathbf{r})\phi_B(\mathbf{r}) - \xi(\mathbf{r})(1-\phi_A(\mathbf{r})-\phi_B(\mathbf{r}))] \tag{2}$$

Here, χ_{AB} denotes the Flory−Huggins parameter, characterizing the repulsive interaction between the A- and B-type segments. The function $\xi(\mathbf{r})$ is Lagrangian multiplier to enforce the incompressibility condition ($\phi_A(\mathbf{r}) + \phi_B(\mathbf{r}) = 1$). Q_G is the partition function of a single noninteracting, grafted chain subject to the chemical potential fields $\omega_A(\mathbf{r})$ and $\omega_B(\mathbf{r})$ in terms of the backbone propagator $q_A(\mathbf{r},s)$. The variable s is proportional to the arc length along the contour of the polymer, where s is scaled by N_A for backbone and N_B for graft chains. The spatial coordinate $\mathbf{r}$ is in units of R_g, where $R_g^2 = N_G a^2/6$. The backbone propagator is divided into $z + 1$ blocks

$$q_A(\mathbf{r},s) = q_A^{(g)}(\mathbf{r},s) \quad \text{for} \quad \tau_g \le s < \tau_{g+1} \quad g = 0, 1, \ldots, z \quad \tau_0 \equiv 1, \quad \tau_{z+1} \equiv 1 \tag{3}$$

where each block satisfies the modified diffusion equation

$$\frac{N_G}{N_A}\frac{\partial q_A^{(g)}(\mathbf{r},s)}{\partial s} = \nabla^2 q_A^{(g)}(\mathbf{r},s) - \omega_A(\mathbf{r})q_A^{(g)}(\mathbf{r},s) \tag{4}$$

The equation is subject to the following initial condition

$$q_A^{(g)}(\mathbf{r},\tau_g) = q_A^{(g-1)}(\mathbf{r},\tau_g^-)q_B(\mathbf{r},1) \qquad g = 1, 2, \ldots, z \qquad q_A^{(0)}(\mathbf{r},0) = 1 \tag{5}$$

where $q_A^{(g-1)}(\mathbf{r}, \tau_g^-)$ is the limit of the function as s approaches τ_g from below (just after the junction point). $q_B(\mathbf{r}, s)$ is a

propagator for graft chains, which is the solution of the modified diffusion equation

$$\frac{N_G}{N_B}\frac{\partial q_B(\mathbf{r},s)}{\partial s} = \nabla^2 q_B(\mathbf{r},s) - \omega_B(\mathbf{r}) q_B(\mathbf{r},s) \quad (6)$$

with the initial condition $q_B(\mathbf{r}, 0) = 1$ for the free end of the graft chains at $s = 0$. In terms of the backbone propagator $q_A(\mathbf{r}, s)$, we can compute the single chain partition function

$$Q_G = \int d\mathbf{r} q_A(\mathbf{r}, 1) \quad (7)$$

In addition, we also define a backward propagator of the gth graft chain $\bar{q}_B^{(g)}(\mathbf{r}, s)$, which satisfies the same diffusion equation $q_B(\mathbf{r}, s)$ with the right-hand side multiplied by -1, but starts on the junction point of the graft chain and is subject to the initial condition

$$\bar{q}_B^{(g)}(\mathbf{r}, 1) = q_A^{(g-1)}(\mathbf{r}, \tau_g^-) q_A^{(z-g)}(\mathbf{r}, (1-\tau_g)^-) \quad (8)$$

Minimization of the free energy F, with respect to $\phi_A(\mathbf{r})$, $\phi_B(\mathbf{r})$, $\omega_A(\mathbf{r})$, $\omega_B(\mathbf{r})$, and $\xi(\mathbf{r})$, is achieved by satisfying a set of mean-field equations

$$\omega_A(\mathbf{r}) = \chi_{AB} N_G \phi_B(\mathbf{r}) + \xi(\mathbf{r}) \quad (9)$$

$$\omega_B(\mathbf{r}) = \chi_{AB} N_G \phi_A(\mathbf{r}) + \xi(\mathbf{r}) \quad (10)$$

$$\phi_A(\mathbf{r}) = -\frac{V}{Q_G}\frac{\delta Q_G}{\delta \omega_A(\mathbf{r})} \quad (11)$$

$$\phi_B(\mathbf{r}) = -\frac{V}{Q_G}\frac{\delta Q_G}{\delta \omega_B(\mathbf{r})} \quad (12)$$

$$\phi_A(\mathbf{r}) + \phi_B(\mathbf{r}) = 1 \quad (13)$$

In terms of these propagators, the segment densities $\phi_A(\mathbf{r})$ and $\phi_B(\mathbf{r})$ are given by

$$\phi_A(\mathbf{r}) = \frac{V f_A}{Q_G}\sum_{g=0}^{z}\int_{\tau_g}^{\tau_{g+1}} ds q_A^{(g)}(\mathbf{r}, s) q_A^{(z-g)}(\mathbf{r}, 1-s) \quad (14)$$

$$\phi_B(\mathbf{r}) = \frac{V f_B}{m Q_G}\sum_{g=1}^{z}\int_0^1 ds q_B(\mathbf{r}, s) \bar{q}_B^{(g)}(\mathbf{r}, s) \quad (15)$$

In our previous study, the real-space method for numerically solving the SCFT equations was adopted.[52–54] While the method provides an efficient approach to search for the ordered structures, the method tends to be computationally intensive for melt phase with spatial variation in three dimensions. Instead, we use the reciprocal space method invented by Matsen and Schick,[3] which allows for the rapid and very accurate exploration of mean-field thermodynamics. The method utilizes the symmetry properties of the ordered structures. A set of basis functions $f_n(\mathbf{r})$ are used to span the function space and solve $q_A(\mathbf{r}, s)$, $q_B(\mathbf{r}, s)$, and $q_B^{(g)}(\mathbf{r}, s)$ at an arbitrary set of external fields. Details of the reciprocal method of SCFT for graft copolymers are presented in the Appendix.

Results

A. Phase Diagram. The phase diagrams were constructed by comparing the free energies of the different microphase separated structures and choosing the one with the minimal free energy as the equilibrium structure. The free energy for an ordered structure has to be minimized with respect to the periodicity D/R_g of the structure. In the reciprocal space method, the symmetries of the ordered structures are chosen a priori.[55] In our present study, because our main aim is to examine the effect of molecular architecture on the phase behavior of graft copolymers, the stable structures considered include lamella (L), bicontinuous gyroid (G), hexagonally packed cylinders (C), and body-centered cubic spheres (S). In addition, the two-phase coexistence regions around the phase boundaries are neglected in our calculations for simplicity.

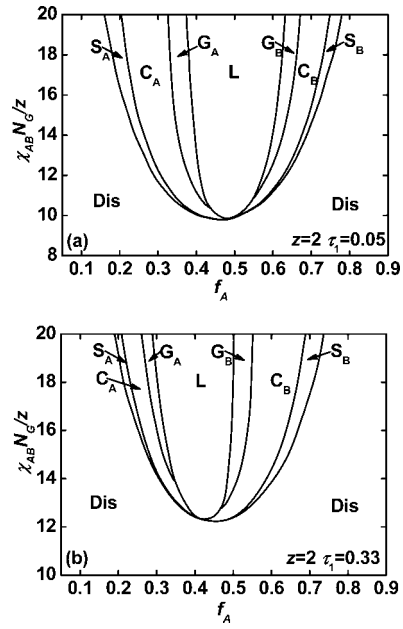

Figure 2. Mean-field phase diagrams for graft copolymers with various molecular architectures (a) $z = 2$, and $\tau_1 = 0.05$; (b) $z = 2$, and $\tau_1 = 0.33$. Dis labels the regions where the melt is disordered. The ordered regions are denoted as S (body-centered cubic spheres, $Im\bar{3}m$ symmetry), C (hexagonally packed cylinders, $P6mm$ symmetry), G (bicontinuous gyroid, $Ia\bar{3}d$ symmetry), and L (Lamella). The solid lines represent the phase boundaries between different phases. The subscript A and B of G, C, and S represent that the minority domains are occupied by the A and B blocks, respectively.

Figure 2 shows the mean-field phase diagrams of graft copolymers with the first junction point $\tau_1 = 0.05$ and $\tau_1 = 0.33$ at the graft number $z = 2$. In the phase diagrams, the vertical axis is the interaction strength $\chi_{AB}N_G/z$ of the average constituting single graft copolymer. The solid lines represent the phase boundaries between different phases. The ordered phases are labeled as L (Lamella), G (Gyroid), C (Cylinder), and S (Sphere). The subscript A and B of G, C, and S represent that the minority domains are occupied by the A and B blocks, respectively. As the volume fraction f_A of backbone increases in the phase diagrams from left to right, the sequence of ordered phases follows: S_A-C_A-G_A-L-G_B-C_B-S_B. One notable feature of these phase diagrams is that they are not symmetrical about $f_A = 0.50$. For $\tau_1 = 0.05$, the phases (S_A, C_A, and G_A) with the backbone blocks in the minority domains occupy a wide range of f_A for a given $\chi_{AB}N_G/z$, while the regions of ordered phases (G_B, C_B, and S_B) with backbone blocks forming the matrix are narrow (as shown in Figure 2a). For $\tau_1 = 0.33$, another scenario is observed in Figure 2b. The regions of phases (G_B, C_B, and S_B) are wider than those of phases (G_A, C_A, and S_A) for a given $\chi_{AB}N_G/z$. The triple points, which are at the intersection of C, G, and L phases, are also not symmetrical. Another feature of the phase diagrams is that the order−disorder transition (ODT) is dramatically altered by the position of the first junction point as can be seen from the comparison between Figure 2a and 2b. The critical point of graft copolymer melts, which indicates a second-order transition from the disordered state to lamellar phase, is shifted when τ_1 changes, for example, $\chi_{AB}N_G/z = 9.91$

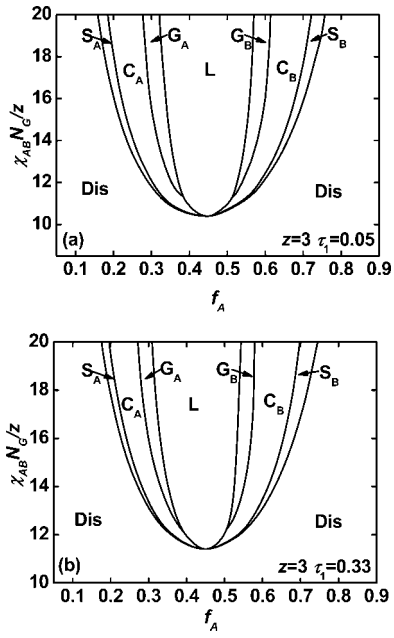

Figure 3. Mean-field phase diagrams for graft copolymers with various molecular architectures (a) $z = 3$, and $\tau_1 = 0.05$; (b) $z = 3$, and $\tau_1 = 0.33$. Labels appear as in Figure 2.

and $f_A = 0.497$ for $\tau_1 = 0.05$; and $\chi_{AB}N_G/z = 12.34$ and $f_A = 0.412$ for $\tau_1 = 0.33$.

The SCFT phase diagrams of graft copolymers with the first junction point $\tau_1 = 0.05$ and $\tau_1 = 0.33$ at $z = 3$ are illustrated in Figure 3. Similarly, the architecture parameters have a significant impact on the phase diagrams of graft copolymers at $z = 3$. The phase diagrams of the graft copolymers at $z = 3$ are also asymmetric. The critical point shifts toward one side of ODT. The triple points also have a shift and are tilted. It can be seen that the regions of stability structures and phase boundaries have a marked change as the graft number increases 2 to 3. Since τ_1 and z exert a marked effect on the phase behavior of the graft copolymers, it is instructive to plot phase diagrams of the graft copolymer melts, in which the first junction position (τ_1) or graft number (z) versus the volume fraction of backbone (f_A) plane is plotted at a fixed degree of segregation ($\chi_{AB}N_G/z$).

Phase diagrams in τ_1 versus f_A space for graft copolymers with $z = 2$ and $z = 3$ at $\chi_{AB}N_G/z = 18.0$ are shown in Figure 4. The ordered phase region tends to be narrow at the intermediate values of τ_1. The stable regions of S_A, C_A, and G_A, where the backbone blocks form the minority domains, have a minimum at the intermediate values of τ_1. However, the stable regions of S_B, C_B, and G_B, where the backbone blocks produce the matrix, have a maximum at the intermediate values of τ_1. There are strong shifts in boundaries of order-order transitions (OOTs) first to the left and then to the right as the τ_1 value increases except for S_A-C_A boundary. In the region of smaller τ_1, the boundaries of OOTs tend to shift toward smaller values of f_A with increasing the value of τ_1. In the region of larger τ_1, increasing the τ_1 value gives rise to the shift toward larger values of f_A. In the region of intermediate τ_1, the effect of τ_1 on the boundaries of OOTs is not significant. The shifts of OOTs induced by variation of the first junction position can result in some novel transition sequences, which is different from the transition order induced by the volume fraction of backbone. For example, the transition sequence of L-G_B-C_B-G_B-L is triggered by changing the first junction position τ_1 from zero to 0.5 at $z = 2$, $f_A = 0.58$, and $\chi_{AB}N_G/z = 18.0$, which is traced out by an arrow in Figure 4a.

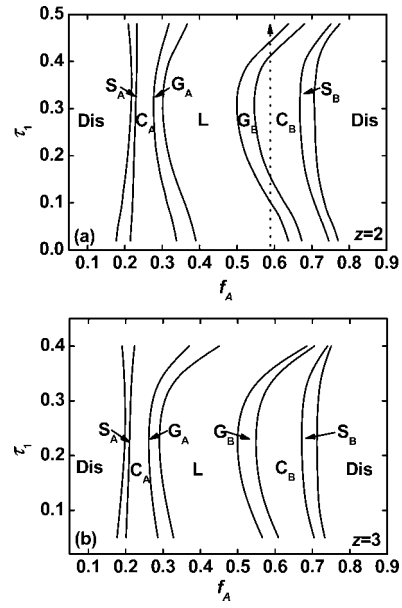

Figure 4. Mean-field phase diagrams in τ_1-f_A space for graft copolymers with (a) $z = 2$ and (b) $z = 3$ at $\chi_{AB}N_G/z = 18.0$. Labels appear as in Figure 2.

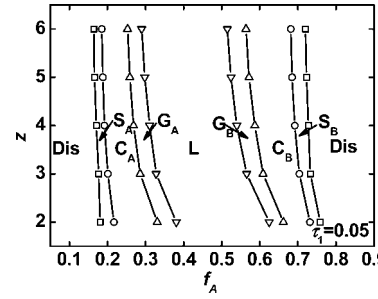

Figure 5. Mean-field phase diagram in z-f_A space for graft copolymers with $\tau_1 = 0.05$ at $\chi_{AB}N_G/z = 18.0$. Labels appear as in Figure 2.

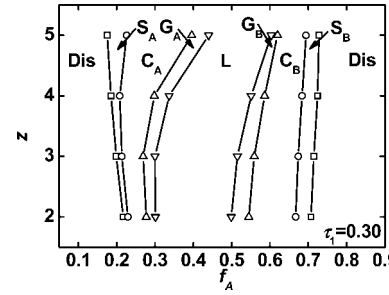

Figure 6. Mean-field phase diagram in z-f_A space for graft copolymers with $\tau_1 = 0.30$ at $\chi_{AB}N_G/z = 18.0$. Labels appear as in Figure 2.

From Figure 4a and 4b, the influence of graft number on phase behavior can also be viewed. In the region of smaller τ_1, the phase boundaries tend to shift toward smaller values of f_A as z increases from 2 to 3. In the region of larger τ_1, the phase boundaries tend to shift toward larger values of f_A with increasing z. In the region of intermediate τ_1, the effect of z on the phase boundaries is not marked. The effect of graft number on phase behavior in the smaller, larger, intermediate regions of τ_1 can be further viewed in Figures 5, 6, and 7, respectively.

Figure 5 illustrates the mean-field phase diagram in z-f_A space for graft copolymers with $\tau_1 = 0.05$ at $\chi_{AB}N_G/z = 18.0$. For graft copolymers with $z = 2$ and $z = 3$, the stable ordered phase regions including S_A, C_A, and G_A, where the backbone blocks form the minority domain, are broader than those of their

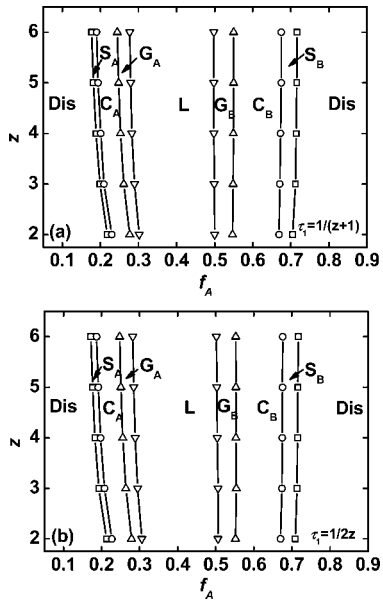

Figure 7. Mean-field phase diagrams in z-f_A space for graft copolymers with (a) $\tau_1 = 1/(z + 1)$ and (b) $\tau_1 = 1/2z$ at $\chi_{AB}N_G/z = 18.0$. Labels appear as in Figure 2.

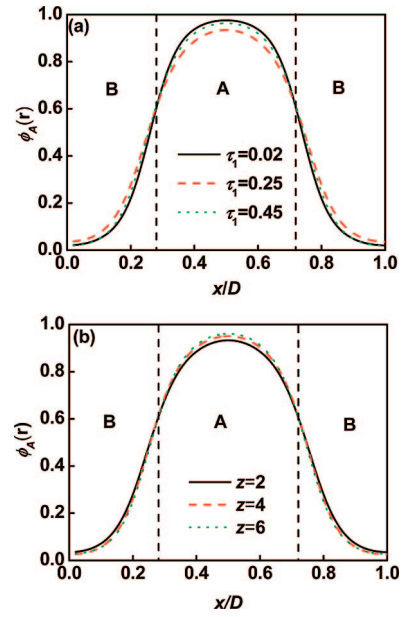

Figure 8. (a) A-segment volume fraction profiles in lamellar phase for graft copolymers with $\tau_1 = 0.02$ (full line), 0.25 (dash line), and 0.45 (dot line) at $z = 2$, $\chi_{AB}N_G/z = 18.0$, and $f_A = 0.48$. The equilibrium length scales D are $2.89R_g$, $2.45R_g$, and $2.74R_g$, for $\tau_1 = 0.02$, 0.25, and 0.45, respectively. (b) A-segment volume fraction profiles in lamellar phase for graft copolymers with $z = 2$ (full line), 4 (dash line), and 6 (dot line) at $\tau_1 = 0.30$, $\chi_{AB}N_G/z = 18.0$, and $f_A = 0.48$. The equilibrium length scales D are $2.44R_g$, $1.87R_g$, and $1.66R_g$, for $z = 2$, 4, and 6, respectively.

corresponding reverse phases. An increase in the number of grafts shrinks the phase regions (S_A, C_A, and G_A) but enlarges the regions of their corresponding reverse phases. As z is above 4, the phases (S_B, C_B, and G_B) with the backbone blocks outside of curved interfaces are favored. The OOTs shift toward the smaller f_A values when z increases from 2 to 6.

Figure 6 displays the phase diagram plotted in z versus f_A plane for graft copolymers with larger τ_1 value at fixed $\chi_{AB}N_G/z = 18.0$.The stability regions of morphologies (S_A, C_A, and G_A) with backbone in the inside of curved interface are suppressed at $z = 2$. However, the stability regions of these phases are enlarged because of the additional asymmetry introduced by increasing the graft number. The ordered phases with backbone in the inside of the curved interface are favored at $z = 5$. The volume fractions of OOTs tend to shift toward the larger values of f_A as z increases.

As for the influence of graft number at the intermediate value of τ_1, two cases in terms of the junction distribution are calculated. On is that τ_1 is set to be $1/(z + 1)$. Under this condition, the length of inner blocks between neighbor junctions is equal to that of free end blocks. The other case is that τ_1 is taken to be $1/(2z)$. With this adoption of τ_1, the constituting block copolymers by cutting the middle point of the connecting blocks are the symmetric single graft architectures. Figure 7 shows the z-f_A phase diagrams for graft copolymers with $\tau_1 = 1/(z+1)$ and $\tau_1 = 1/(2z)$ at $\chi_{AB}N_G/z = 18.0$. The phases (S_B, C_B, and G_B) with the backbone blocks in the outside of curved interface are more favored. The phase boundaries of L-G_B, G_B-C_B, and C_B-S_B are almost invariable as the graft number changes. However, the phase boundaries of S_A-C_A, C_A-G_A, and G_A-L have a slight shift toward smaller values of f_A as the graft number increases. The different between panels a and b in Figure 7 is small. This can also be viewed in Figure 4 that the effect of τ_1 on the phase boundaries of graft copolymers is not marked at intermediate values of τ_1.

B. Density Distribution and Domain Spacing. A useful feature of SCFT is that it yields the density distribution and domain spacing, which are associated with the various properties of graft copolymers. Figure 8a shows the A-segment volume fraction profiles in lamellar phase for graft copolymers with $\tau_1 = 0.02$, 0.25, and 0.45 at $z = 2$, $\chi_{AB}N_G/z = 18.0$, and $f_A = 0.48$. In comparison with τ_1 at larger or smaller values, a slight decrease in segregation occurs when τ_1 values are in the intermediate range. Figure 8b displays the A-segment volume fraction profiles in lamellar phase for graft copolymers with $z = 2$, 4, and 6. A slight increase in segregation takes place as z increases. In comparison with the thermodynamic parameters (volume fraction of block and degree of segregation), the architecture parameters of copolymers has a weak impact on the density distribution of graft copolymers.

Figure 9a illustrates the period D/R_g of the lamellar phase as a function of the first junction position at $f_A = 0.48$ and $\chi_{AB}N_G/z = 18.0$ for $z = 2$ and 3. At smaller τ_1 values, D/R_g decreases with increasing τ_1. As τ_1 increases, the change in D/R_g becomes less marked. With further increasing τ_1, D/R_g increases. It is also noted that the lamellar phase period of the graft copolymers with smaller z is greater than that having larger z. When τ_1 is smaller, the domain spacing is mainly controlled by the length of inner blocks. The length of inner blocks becomes shorter, and the domain spacing decreases with an increase in τ_1. When τ_1 is in the intermediate range, the period of lamellar phase reaches a minimum. The period slowly changes at the intermediate range of τ_1 because of the competition between the lengths of free end blocks and inner blocks. When τ_1 is larger, the free end blocks are the longest ones that determine the domain spacing. As τ_1 further increases, the domain spacing has a significant increase. Figure 9b shows the lamellar period D/R_g as a function of the number of grafts at $f_A = 0.48$ and $\chi_{AB}N_G/z = 18.0$ for $\tau_1 = 0.05$ and $\tau_1 = 0.30$. Increasing the graft number gives rise to a decrease in the domain spacing. This trend can be ascribed to the fact that the average lengths of graft chains and backbone blocks become short as the graft number increases.

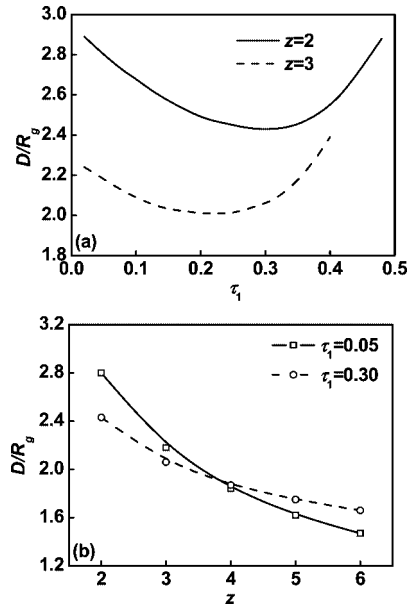

Figure 9. (a) Lamellar period D/R_g as a function of the first junction position τ_1 at $f_A = 0.48$ and $\chi_{AB}N_G/z = 18.0$ for $z = 2$ and $z = 3$. (b) Lamellar period D/R_g as a function of the graft number z at $f_A = 0.48$ and $\chi_{AB}N_G/z = 18.0$ for $\tau_1 = 0.05$ and $\tau_1 = 0.30$.

Discussion

Although the topology of the phase diagrams for graft copolymers is equivalent to that of the standard AB diblock copolymer melts, SCFT predicts several significant differences (as shown Figures 2 and 3). For the classic phase diagram of diblock copolymers,[3] it is plotted in $\chi_{AB}N$-f_A space and is symmetric about $f_A = 0.50$. With respective to the graft copolymers, the vertical axis of phase diagrams is the interaction strength $\chi_{AB}N_G/z$ of the average constituting single graft copolymers. Because of the additional asymmetry introduced by molecular architecture, change from the diblock copolymers to graft copolymers breaks the $f_A \leftrightarrow 1 - f_A$ symmetry of the phase diagrams. The phase behavior of diblock copolymers is determined by the copolymer composition and segregation degree. For the graft copolymers, in addition to these two parameters, the architecture parameters (the graft number and junction distribution) exert a significant effect on the phase boundaries and stability regions of phase diagrams.

Another distinct difference between diblock copolymers and graft copolymers is that the graft copolymers have junctions along the backbone constrained to the domain interfaces. The backbone blocks of graft copolymers can take either looped conformation whose neighbor junctions locate in the same domain or bridged conformation whose neighbor junctions are anchored on the different domain interfaces. The existence of bridged blocks linking separate domains strongly affects the mechanical properties of the graft copolymers at fracture. Therefore, the fraction of bridged conformation is a crucial parameter for material design. In our previous study, we have investigated the bridged and looped conformation of the backbone of the graft copolymer by using self-consistent field theory.[52] The fraction of bridged conformation has a tendency to decrease with increasing the length of free end blocks and the number of grafts. The number of bridged chains per unit area increases with increasing the number of grafts in the cylindrical phase. But in the lamellar phase, it decreases when the graft number increases.

The phase diagrams of graft copolymer melts strongly depend on the first junction position and graft number (as shown in Figures 4–7). This behavior can be rationalized by considering the stretching energy of the chains. The backbone of graft copolymers is composed of two different length blocks (free end blocks and inner blocks). The graft copolymers with a smaller τ_1 (larger τ_1) value have the longer length of inner (free end) blocks. The availability of longer and shorter blocks capable of filling the interstitial regions can relieve the excessive stretching and compression (as shown in Figure 10a and 10c). When τ_1 becomes intermediate, the asymmetry of free and inner blocks of backbone becomes small and the blocks become overcrowded. Since the polymer chains must be adjusted to maintain a constant density for an incompressible system,[45] the free end blocks and inner blocks have to be stretched away from the interface and compressed close to the interface. The lateral crowding and additional chain stretching can be partially alleviated by allowing the interface to curve away form backbone domain. These result in an enhanced preference for backbone to remain on the convex side of the interface, which is illustrated in Figure 10b. Such a preference causes the shifts of OOT lines toward lower backbone block volume fraction in the intermediate region of τ_1 (as shown in Figure 4).[16]

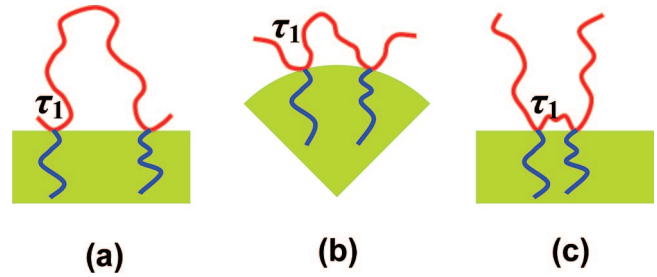

Figure 10. Schematic representations of graft copolymers on an interface. (a) Graft copolymer with a smaller value of τ_1 at a flat interface; (b) graft copolymer with a intermediate value of τ_1 at a curved interface; (c) graft copolymer with a larger value of τ_1 at a flat interface. The curvature interface is exaggerated.

Similarly, the inner blocks become overcrowded because of the junction constraint of the backbone as the graft number increases (fixed the τ_1 at smaller value). To alleviate the crowding and stretching of inner blocks and lower the total free energy, the interface curves away from backbone domain. This change in the spontaneous curvature shifts the OOTs toward smaller f_A as the graft number increases (Figure 5). The graft copolymers with larger τ_1 values, which have the shorter length of inner blocks, can be regarded as the star copolymers. The graft chains become overcrowded as the graft number increases. Consequently, the interface curves away from graft chain domain. This results in the shifts in OOTs toward the larger f_A values as the graft number increases (as shown in Figure 6). At intermediate τ_1 values, the phase boundaries of OOTs tend to be invariable as the graft number increases (as shown in Figure 7), because the length difference of free end blocks and inner blocks is small.

Some experimental evidence are available in the literature, supporting the predicted results of SCFT for graft copolymer melts. Gido et al. synthesized a series of well-defined graft copolymers with polyisoprene (PI) backbone and polystyrene (PS) branches (PS-*g*-PI).[14–21] They can precisely control over the backbone molecular weight, arm molecular weight, arm polydispersity, and placement of junction points, etc. The microphase separation of graft copolymers was observed, and the classical microdomian geometries of lamella, cylinder, and sphere were identified.

For comparison with the experiments, we calculated the phase diagram of graft copolymers at strong segregation in accord

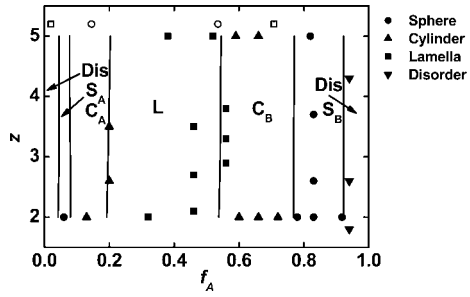

Figure 11. Comparison of the SCFT results with the experimental findings at strong segregation. The solid lines represent the phase boundaries between different phases obtained from the SCFT calculation of graft copolymers with $\tau_1 = 1/2z$ at $\chi_{AB}N_G/z = 80.0$. The filled symbols indicate the results from the experiments of polystyrene-*g*-polyisoprene graft copolymer melts.[16,17,21] (■) Lamellar phase, (▲) cylindrical phase, (●) spherical phase, and (▼) disordered state. The hollow symbols represent the transition points between different phases calculated according to Milner's theory.[22] (□) S−C transitions, and (○) C−L transitions.

with the strong incompatibility of PS and PI.[17] Because of the numerical difficulties of the considered gyroid phase for large $\chi_{AB}N_G/z$, the gyroid phase is not included in the phase diagram. In our calculations, the boundaries of disorder−sphere, sphere−cylinder, and cylinder−lamella transitions are evaluated. Figure 11 illustrates the SCFT z-f_A phase diagram of graft copolymers with $\tau_1 = 1/(2z)$ at $\chi_{AB}N_G/z = 80.0$. The phase boundaries calculated by SCFT are represented by the solid lines. In Figure 11, the results from the experiments of graft copolymers with regularly spaced junction points are also presented.[16,17,21] The vertical and horizontal axes of phase diagram correspond to the number of junction points per molecule and the volume fraction of polyisoprene in experiments, respectively. The filled symbols in Figure 11 indicate the experimentally observed morphologies. Our phase diagram calculated by SCFT is in good agreement with the experimental results of PS-*g*-PI graft copolymer melts. One exception is that the lamellar phases formed by graft copolymers with 56 vol% PI are located in the cylindrical phase region of theoretical phase diagram. But the discrepancy between the experiment and prediction is small. Such a difference could be attributed to a number of factors associated with our simple model (not consider the fluctuation effects, actual sizes of the monomers, and the random distribution of junction points) and sample polydispersity.

As for the theoretical considerations of the phase behavior of graft copolymers, Gido et al. prescribed an empirical method.[14–21] It was proposed that the morphologies of graft copolymers are governed by the behavior of constituting block copolymers, which is a single-graft architecture by cutting the connecting blocks of backbone at the middle. The single-graft copolymers can be regarded as A_2B star architecture. Existing Milner's theory in strong segregation limit is used to capture the phase behavior of A_nB_m star copolymers.[22] This theory predicts the phase boundaries as functions of the component volume fraction and molecular asymmetry parameter. For the PS-*g*-PI graft copolymers studied by Gido et al., the molecular asymmetry parameter of single-graft copolymers was calculated to be 1.78.[15] The sphere−cylinder and cylinder−lamella transition points calculated by Milner's theory are also presented in the phase diagram (as shown in Figure 11). The general tendency of Milner's predictions is in agreement with the experimental results. However, in comparison with our calculations, the Milner's prediction has some degree of overestimation, especially in the phase regions where the minority domains are formed by the backbone. The reason for the overestimation could be ascribed to a junction point delocalization effect at the AB interface, which is neglected in Milner's calculations.[16] In real case, the junction points of A and B blocks may delocalize from the interface,[47] while in Milner's theory they are assumed to be confined to the interface. As can been seen from above discussion, SCFT in comparison with the Milner's theory can more accurately capture the characteristics of the phase behaviors of the graft copolymers.

Conclusion

In this study, we examined the phase behavior of graft copolymer melts using the reciprocal-space self-consistent field theory. The $\chi_{AB}N_G/z$-f_A space phase diagrams for graft copolymers with various molecular architectures were constructed by comparing the computed free energy of different phases. In comparison with the AB diblock copolymers, the phase boundaries become asymmetric about $f_A = 0.50$. We also mapped out the phase diagrams of τ_1-f_A space and z-f_A space. There are shifts in phase boundaries of OOTs first to the smaller values of f_A and then to the larger values of f_A as the first junction position τ_1 changes from zero to 0.5. In the region of smaller τ_1, the boundaries of OOTs shift toward the smaller values of f_A as the graft number z increases. In the region of larger τ_1, the boundaries of OOTs shift toward the larger values of f_A with increasing the graft number. In the region of intermediate τ_1, the shifts of phase boundaries are small when the graft number changes. In addition, the molecular architecture of graft copolymers significantly alters the domain spacing of ordered structures but has weak impact on the density profiles of respective components.The theoretical results obtained by the self-consistent field theory calculations in the strong segregation were compared with the existing experimental findings, and a good agreement was found.

Acknowledgment. This work was supported by National Natural Science Foundation of China (50673026, 20574018). Support from Doctoral Foundation of Education Ministry of China (Grant No. 20050251008), Program for New Century Excellent Talents in University in China (NCET-04-0410), and Projects of Shanghai Municipality (06SU07002, 0652nm021, 082231, and B502) are also appreciated.

Appendix. Spectral Solution to SCFT Equations

In this appendix, we present details of numerical solution to SCFT equations in reciprocal space. For a periodic ordered phase, all functions of position vector **r** are expanded in a Fourier-like series

$$g(\mathbf{r}) = \sum_i g_i f_i(\mathbf{r}) \tag{A1}$$

The appropriate basis functions for the expansion are the eigenfunctions $f_i(\mathbf{r})$ of Laplace operator

$$\nabla^2 f_i(\mathbf{r}) = -\frac{\lambda_i}{D^2} f_i(\mathbf{r}) \tag{A2}$$

where D is the length scale of the periodicity of the system. By convention, $f_0(\mathbf{r}) = 1$ (or $\lambda_1 = 0$), and the eigenfunctions are ordered in an nondecreasing sequence of λ_i. In addition, the set of functions are normalized

$$\frac{1}{V}\int \mathrm{d}\mathbf{r} f_i(\mathbf{r}) f_j(\mathbf{r}) = \delta_{ij} \tag{A3}$$

We can also write the product of two basis functions ($f_i(\mathbf{r})$ $f_j(\mathbf{r})$) as expansion in our basis functions

$$f_i(\mathbf{r}) f_j(\mathbf{r}) = \sum_k \Gamma_{ijk} f_k(\mathbf{r}) \tag{A4}$$

Here, Γ_{ijk} is the coefficient of the expansion. Alternately, those coefficients can be computed by $\Gamma_{ijk} = V^{-1}\int d\mathbf{r}\, f_i(\mathbf{r})\, f_j(\mathbf{r}) f_k(\mathbf{r})$.

With these definitions and the Fourier expansions of functions, the partial differential equation becomes a differential equation form

$$\frac{\mathrm{d}q_{\mathrm{B},i}(s)}{\mathrm{d}s} = \sum_j \mathrm{B}_{ij} q_{\mathrm{B},j}(s) \tag{A5}$$

where the matrix B is given by $B_{ij} = (-\lambda_i \delta_{ij}/D^2 - \sum_k \omega_{\mathrm{B},k}\Gamma_{ijk})N_\mathrm{B}/N_\mathrm{G}$, and the initial condition is $q_{\mathrm{B},i}(0) = \delta_{i1}$. The solution to the set of linear differential equations is

$$q_{\mathrm{B},i}(s) = T_{\mathrm{B},i1}(s) \tag{A6}$$

where $T_\mathrm{B}(s') = \exp(\mathrm{B}s')$ is the matrix that transfers $q_{\mathrm{B},i}(s)$ a distance s' along the graft chain. Since the matrix B is symmetric and real, the matrix can be computed by performing an orthogonal transformation that diagonalizes B, such that $\mathrm{B} = U_\mathrm{B}\Lambda_\mathrm{B}U_\mathrm{B}^T$, where $\Lambda_\mathrm{B} = \mathrm{diag}(\lambda_{\mathrm{B},1},\lambda_{\mathrm{B},2},..., \lambda_{\mathrm{B},n})$ is the eigenvalues of B, $U_\mathrm{B} = \{u_{\mathrm{B},1},u_{\mathrm{B},2},..., u_{\mathrm{B},n}\}$ is the eigenvectors of B. Therefore,

$$T_{\mathrm{B},ij}(s) = \sum_k u_{\mathrm{B},ik}\exp(\lambda_{\mathrm{B},k}s)u^T_{\mathrm{B},kj} \tag{A7}$$

Similarly, the diffusion equation for $q_\mathrm{A}(\mathbf{r}, s)$ becomes

$$\frac{\mathrm{d}q^{(g)}_{\mathrm{A},i}(s)}{\mathrm{d}s} = \sum_j \mathrm{A}_{ij} q^{(g)}_{\mathrm{A},i}(s) \tag{A8}$$

where $\mathrm{A}_{ij} = (-\lambda_i\delta_{ij}/D^2 - \sum_k \omega_{\mathrm{A},k}\Gamma_{ijk})N_\mathrm{A}/N_\mathrm{G}$. The solution for $q_\mathrm{A}(\mathbf{r}, s)$ is given by

$$q^{(g)}_{\mathrm{A},i}(s) = T_{\mathrm{A},ij}(s-\tau_g)q^{(g)}_{\mathrm{A},j}(\tau_g) \tag{A9}$$

where $T_\mathrm{A}(s - \tau_g) = \exp(\mathrm{A}(s - \tau_g))$ is a matrix that transfers the solution from τ_g to s for the backbone. To evaluate the matrix, we diagonalize A by orthogonal transformation, such that $\mathrm{A} = U_\mathrm{A}\Lambda_\mathrm{A}U_\mathrm{A}^T$, where $\Lambda_\mathrm{A} = diag(\lambda_{\mathrm{A},1},\lambda_{\mathrm{A},2},..., \lambda_{\mathrm{A},n})$ is the eigenvalues of A, $U_\mathrm{A} = \{u_{\mathrm{A},1},u_{\mathrm{A},2},..., u_{\mathrm{A},n}\}$ is the eigenvectors of A. Using these matrixes, we can write the solution

$$q^{(g)}_{\mathrm{A},i}(s) = u_{\mathrm{A},ik}\exp(\lambda_{\mathrm{A},k}(s-\tau_g))u^T_{\mathrm{A},kj}q^{(g)}_{\mathrm{A},j}(\tau_g) \tag{A10}$$

where $q^{(g)}_{\mathrm{A},i}(\tau_g)$ are the boundary conditions for $q^{(g)}_{\mathrm{A},i}(s)$ at τ_g

$$q^{(g)}_{\mathrm{A},i}(\tau_g) = \sum_{j,k} q^{(g-1)}_{\mathrm{A},j}(\tau_g^-)q_{\mathrm{B},k}(1)\Gamma_{ijk} \qquad g = 1, 2, \ldots, z \tag{A11}$$

We use the fact that $q^{(0)}_{\mathrm{A},i}(0) = \delta_{i1}$, which is the boundary condition for the free end, is used to compute $q^{(0)}_{\mathrm{A},i}(s)$. We can then use eq A11 along $q^{(0)}_{\mathrm{A},i}(\tau_g^-)$ and $q_{\mathrm{B},k}(1)$ to find $q^{(1)}_{\mathrm{A},i}(s)$ for the block between τ_1 and τ_2. Repeating this process, we can find $q^{(g)}_{\mathrm{A},i}(\tau_g)$ and $q^{(g)}_{\mathrm{A},i}(s)$ for all blocks. In addition, we also can compute the single-chain partition function $Q = Vq_{\mathrm{A},1}(1)$.

To obtain $\bar{q}^{(g)}_{\mathrm{B},i}(s)$, we solve the same matrix equations as eq A5 with a plus sign on the right-hand side. The solution for $\bar{q}^{(g)}_{\mathrm{B},i}(s)$ is

$$\bar{q}^{(g)}_{\mathrm{B},i}(s) = u_{\mathrm{B},ik}\exp(\lambda_{\mathrm{B},k}(1-s))u^T_{\mathrm{B},kj}\bar{q}^{(g)}_{\mathrm{B},j}(1) \tag{A12}$$

where $\bar{q}^{(g)}_{\mathrm{B},j}(1)$ are the boundary conditions of junction points given by

$$\bar{q}^{(g)}_{\mathrm{B},j}(1) = \sum_{j,k} q_{\mathrm{A},j}(\tau_g^-)q_{\mathrm{A},k}((1-\tau_g)^-)\Gamma_{ijk} \tag{A13}$$

Once $q^{(g)}_{\mathrm{A},i}(s)$, $q_{\mathrm{B},i}(s)$, and $\bar{q}^{(g)}_{\mathrm{B},i}(s)$ are solved with respect to $\omega_{\mathrm{A},i}$ and $\omega_{\mathrm{B},i}$, the Fourier amplitudes of the segment densities $\phi_{\mathrm{A},i}$ and $\phi_{\mathrm{B},i}$ can be given by

$$\phi_{\mathrm{A},i} = \frac{f_A}{q_{\mathrm{A},1}(1)}\sum_{g=0}^{z}\int_{\tau_g}^{\tau_{g+1}}\mathrm{d}s\sum_{j,k} q^{(g)}_{\mathrm{A},j}(s)q^{(z-g)}_{\mathrm{A},k}(1-s)\Gamma_{ijk} \tag{A14}$$

$$\phi_{\mathrm{B},i} = \frac{f_\mathrm{B}}{mq_{\mathrm{A},1}(1)}\sum_{g=1}^{z}\int_0^1 \mathrm{d}s\sum_{j,k} q_{\mathrm{B},j}(s)\bar{q}^{(g)}_{\mathrm{B},k}(s)\Gamma_{ijk} \tag{A15}$$

Finally, the free energy per chain is

$$\frac{F}{n_\mathrm{G}k_\mathrm{B}T} = -\ln q_{\mathrm{A},1}(1) - \chi_{\mathrm{AB}}N_\mathrm{G}\sum_i \phi_{\mathrm{A},i}\phi_{\mathrm{B},i} \tag{A16}$$

For the disordered phase, the free energy reads $F/n_\mathrm{G}k_\mathrm{B}T = \chi_{\mathrm{AB}}N_\mathrm{G}f_\mathrm{A}f_\mathrm{B}$.

We adjust the assumed amplitudes $\omega_{\mathrm{A},i}$ and $\omega_{\mathrm{B},i}$ of the fields, so that the densities calculated above satisfy the self-consistency relations

$$\omega_{\mathrm{A},i} - \omega_{\mathrm{B},i} = \chi_{\mathrm{AB}}N_\mathrm{G}(\phi_{\mathrm{B},i} - \phi_{\mathrm{A},i}) \tag{A17}$$

$$\phi_{\mathrm{A},i} + \phi_{\mathrm{B},i} = \delta_{i1} \tag{A18}$$

The set of SCFT equations are highly nonlinear because the segment density amplitudes, $\phi_{\mathrm{A},i}$ and $\phi_{\mathrm{B},i}$, depend functionally on the field amplitudes, $\omega_{\mathrm{A},i}$ and $\omega_{\mathrm{B},i}$. For some initial values of $\omega_{\mathrm{A},i}$ and $\omega_{\mathrm{B},i}$, the segment density amplitudes, $\phi_{\mathrm{A},i}$ and $\phi_{\mathrm{B},i}$ are computed by eqs A14 and A15, respectively. Then, $\omega_{\mathrm{A},i}$ and $\omega_{\mathrm{B},i}$ can be updated by Anderson mixing scheme.[56] The above computation procedure is repeated until the self-consistent solution is found. The free energy of the ordered phase has to be minimized with respect to the periodicity of the structure. The phase diagrams are obtained by comparing the free energies of different structures and choosing the one with the minimal free energy as the equilibrium structures.

References and Notes

(1) Leibler, L. *Macromolecules* **1980**, *13*, 1602.
(2) Semenov, A. N. *Sov. Phys. JETP* **1985**, *61*, 733.
(3) Matsen, M. W.; Schick, M. *Phys. Rev. Lett.* **1994**, *72*, 2660.
(4) Hamley, I. W. *The Physics of Block Copolymers*; Oxford University Press: New York, 1998.
(5) Bates, F. S.; Fredrickson, G. H. *Phys. Today* **1999**, *52*, 32.
(6) Hadjichristidis, N.; Iatrou, H.; Pitsikalis, M.; Pispas, S.; Avgeropoulos, A. *Prog. Polym. Sci.* **2005**, *30*, 725.
(7) Hadjichristidis, N.; Iatrou, H.; Pitsikalis, M.; Mays, J. W. *Prog. Polym. Sci.* **2006**, *31*, 1068.
(8) Pitsikalis, M.; Pispas, S.; Mays, J. W.; Hadjichristidis, N. *Adv. Polym. Sci.* **1998**, *135*, 1.
(9) Hadjichristidis, N.; Pispas, S.; Pitsikalis, M.; Iatrou, H.; Vlahos, C. *Adv. Polym. Sci.* **1999**, *142*, 71.
(10) Hadjichristidis, N.; Pitsikalis, M.; Iatrou, H. *Adv. Polym. Sci.* **2005**, *189*, 1.
(11) Gersappe, D.; Irvie, D.; Balazs, A. C.; Liu, Y.; Sokolov, J.; Rafailovich, M.; Schwarz, S.; Peiffer, D. G. *Science* **1994**, *265*, 1072.
(12) Kennedy, J. P.; Delvaux, J. M. *Adv. Polym. Sci.* **1991**, *38*, 141.
(13) Kennedy, J. P. In *Thermoplastic Elastomers*; Legge, N. R., Holden, G., Quirk, R., Schroeder, H. E., Eds.; Hanser: Munich, 1996.
(14) Gido, S. P.; Lee, C.; Pochan, D. J.; Pispas, S.; Mays, J. W.; Hadjichristidis, N. *Macromolecules* **1996**, *29*, 7022.

(15) Lee, C.; Gido, S. P.; Poulos, Y.; Hadjichristidis, N.; Tan, N. B.; Trevino, S. F.; Mays, J. W. *J. Chem. Phys.* **1997**, *107*, 6460.
(16) Lee, C.; Gido, S. P.; Poulos, Y.; Hadjichristidis, N.; Tan, N. B.; Trevino, S. F.; Mays, J. W. *Polymer* **1998**, *39*, 4631.
(17) Xenidou, M.; Beyer, F. L.; Hadjichristidis, N.; Gido, S. P.; Tan, N. B. *Macromolecules* **1998**, *31*, 7659.
(18) Beyer, F. L.; Gido, S. P.; Buschl, C.; Iatrou, H.; Uhrig, D.; Mays, J. W.; Chang, M. Y.; Garetz, B. A.; Balsara, N. P.; Tan, N. B.; Hadjichristidis, N. *Macromolecules* **2000**, *33*, 2039.
(19) Weidisch, R.; Gido, S. P.; Uhrig, D.; Iatrou, H.; Mays, J. W.; Hadjichristidis, N. *Macromolecules* **2001**, *34*, 6333.
(20) Zhu, Y.; Weidisch, R.; Gido, S. P.; Velis, G.; Hadjichristidis, N. *Macromolecules* **2002**, *35*, 5903.
(21) Zhu, Y.; Burgaz, E.; Gido, S. P.; Staudinger, U.; Weidisch, R.; Uhrig, D.; Mays, J. W. *Macromolecules* **2006**, *39*, 4428.
(22) Milner, S. T. *Macromolecules* **1994**, *27*, 2333.
(23) Olvera de la Cruz, M.; Sanchez, I. C. *Macromolecules* **1996**, *19*, 2501.
(24) Shinozaki, A.; Jasnow, D.; Balazs, A. C. *Macromolecules* **1994**, *27*, 2496.
(25) Foster, D. P.; Jasnow, D.; Balazs, A. C. *Macromolecules* **1995**, *28*, 3450.
(26) Qi, S.; Chakraborty, A. K.; Wang, H.; Lefebvre, A. A.; Balsara, N. P.; Shakhnovich, E. I.; Xenidou, M.; Hadjichristidis, N. *Phys. Rev. Lett.* **1999**, *82*, 2896.
(27) Qi, S.; Chakraborty, A. K.; Balsara, N. P. *J. Chem. Phys.* **2001**, *115*, 3387.
(28) Qi, S.; Chakraborty, A. K. *J. Chem. Phys.* **2001**, *115*, 3401.
(29) Patel, D. M.; Fredrickosn, G. H. *Phys. Rev. E* **2003**, *68*, 051802.
(30) Ye, X.; Shi, T.; Lu, Z.; Zhang, C.; Sun, Z.; An, L. *Macromolecules* **2005**, *38*, 8853.
(31) Wang, R.; Jiang, Z.; Hu, J. *Polymer* **2005**, *46*, 6201.
(32) Edwards, S. F. *Proc. Phys. Soc.* **1965**, *85*, 613.
(33) Helfand, E. *J. Chem. Phys.* **1975**, *62*, 999.
(34) Helfand, E.; Wasserman, Z. R. *Macromolecules* **1976**, *9*, 879.
(35) Hong, K. M.; Noolandi, J. *Macromolecules* **1981**, *14*, 727.
(36) Vavasour, J. D.; Whitmore, M. D. *Macromolecules* **1992**, *25*, 5477.
(37) Matsen, M. W. *J. Phys.: Condens. Matter* **2002**, *14*, R21.
(38) Matsen, M. W. In *Soft Matter*; Gompper, G., Schick, M., Eds.; Wiley-VCH: Weinheim, Germany, 2005; Vol. 1, p 87.
(39) Matsen, M. W.; Schick, M. *Macromolecules* **1994**, *27*, 6761.
(40) Matsen, M. W.; Thompson, R. B. *J. Chem. Phys.* **1999**, *111*, 7139.
(41) Matsen, M. W. *J. Chem. Phys.* **2000**, *113*, 5539.
(42) Matsen, M. W. *Phys. Rev. Lett.* **2007**, *99*, 148304.
(43) Tyler, C. A.; Qin, J.; Bates, F. S.; Morse, D. C. *Macromolecules* **2007**, *40*, 4654.
(44) Jiang, R.; Jin, Q.; Li, B.; Ding, D.; Shi, A.-C. *Macromolecules* **2006**, *39*, 5891.
(45) Cooke, D. M.; Shi, A,-C. *Macromolecules* **2006**, *39*, 6661.
(46) Grason, G. M.; DiDonna, B. A.; Kamien, R. D. *Phys. Rev. Lett.* **2003**, *91*, 058304.
(47) Grason, G. M.; Kamien, R. D. *Macromolecules* **2004**, *37*, 7371.
(48) Grason, G. M.; Kamien, R. D. *Phys. Rev. E* **2005**, *71*, 051801.
(49) Drolet, F.; Fredrickson, G. H. *Phys. Rev. Lett.* **1999**, *83*, 4317.
(50) Fredrickson, G. H.; Ganesan, V.; Drolet, F. *Macromolecules* **2002**, *35*, 16.
(51) Fredrickosn, G. H. *The Equilibrium Theory of Inhomogeneous Polymers*; Oxford University Press: Oxford, 2006.
(52) Zhang, L.; Lin, J.; Lin, S. *J. Phys. Chem. B* **2007**, *111*, 351.
(53) Zhang, L.; Lin, J.; Lin, S. *J. Phys. Chem. B* **2007**, *111*, 9209.
(54) Zhang, L.; Lin, J.; Lin, S. *Macromolecules* **2007**, *40*, 5582.
(55) *International Tables for X-ray Crystallography*; Henry, N. F. M., Lonsdale, K., Eds.; Kynoch: Birmingham, U. K., 1969; Vol. 1.
(56) Eyert, V. *J. Comput. Phys.* **1996**, *124*, 271.

JP802770Z